

# Fluorescence Lifetime Imaging (FLIM) in Confocal Microscopy Applications: An Overview

Susanne Trautmann, Volker Buschmann, Sandra Orthaus, Felix Koberling, Uwe Ortmann, Rainer Erdmann

PicoQuant GmbH, Rudower Chaussee 29, 12489 Berlin, Germany, info@picoquant.com

## Introduction

During the last two decades, the use of fluorescence in natural sciences has propelled a number of research fields, ranging from biological sciences and applications in the clinical sector (FISH for genetic testing, advanced sequencing technology) to environmental monitoring. In addition, the resulting technological developments have become important in several fields of materials sciences, for example in

characterization of new materials or quality control of semiconductor materials.

The fluorescence lifetime is defined as the time the fluorophor remains in the excited state before returning to the ground state. It is characteristic for every dye and its environment. Additionally, fluorescence lifetime measurements have the advantage to be not influenced by internal settings of the instrument like laser intensity or detector gain.

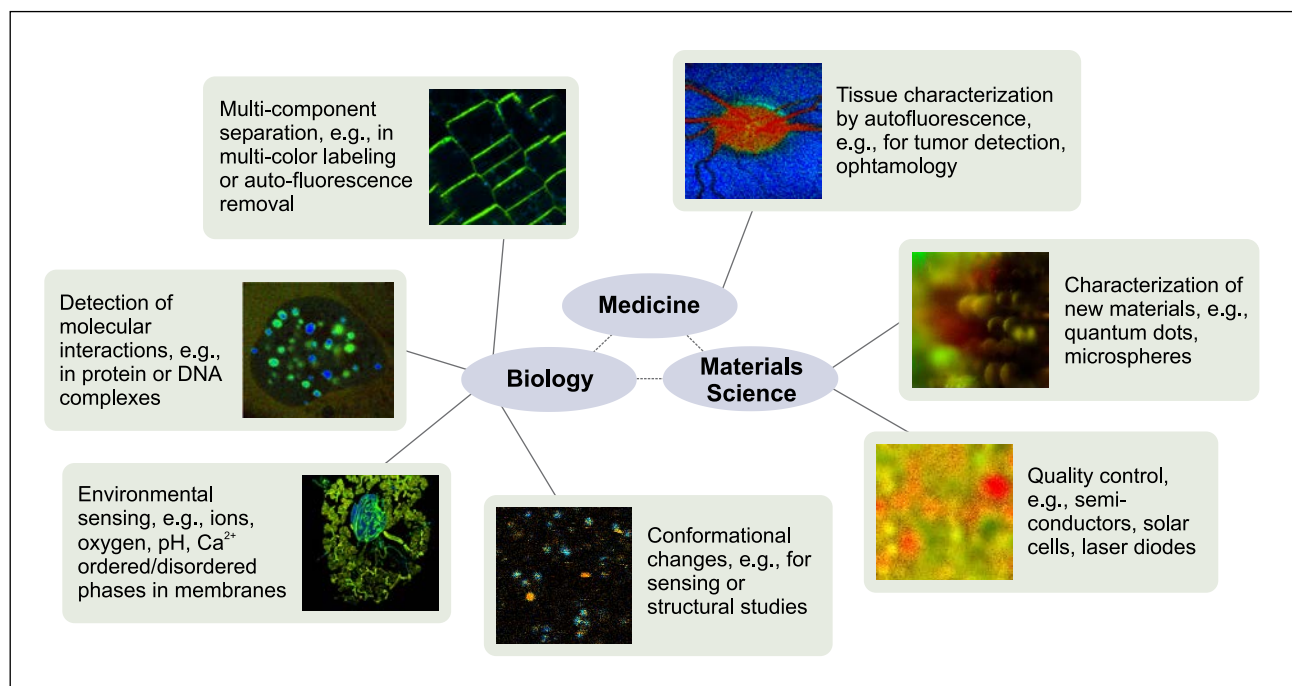


Fig. 1: Applications for FLIM in different scientific fields.

The fluorescence lifetime information is used, e.g., in the following ways:

### 1. Local environment sensing

The fluorescence lifetime can change depending on the fluorophore environment (which means polarity, pH, temperature, ion concentration, etc.) and is therefore used as a parameter for biological sensors. Specifically, fluorophores return to the ground state through radiative and non-radiative processes. Quenching of the excited state by external factors decreases the fluorescence lifetime. The resulting lifetime shortening provides information about the molecular environment of the fluorophore and even allows for quantitative distinction between subpopulations of quenched and unquenched fluorophores.

### 2. Detection of molecular interactions

A special case for the influence of the local environment on fluorescence lifetime is Fluorescence Resonance Energy Transfer (FRET), where the donor dye is quenched by the presence of an acceptor dye. Thus, a decrease of the fluorescence lifetime is indicative for FRET. In this way, the fluorescence lifetime serves as a sensor parameter for intra- and intermolecular interactions allowing for distance measurements in the nanometer range.

### 3. Detection of conformational changes

Applying an intramolecular labelling approach, the distance between the dye and the quencher or FRET acceptor can also vary along with different conformations of the labeled biomolecule. In this way, intramolecular changes, e.g., due to folding or action of molecular motors are detectable.

### 4. Discrimination of multiple labels or background removal

With the advancement of fluorophores and microscopy, researchers now are able to use several fluorescent markers in parallel to assess different processes simultaneously. One challenge is that the employed fluorophores need to be distinguishable and have commonly used spectral characteristics. This limits the number of useful fluorescent markers. The analysis of the fluorescence lifetime can help to overcome these limitations. Additionally, the fluorescence lifetime enables to discriminate label fluorescence from the fluorescence background of the sample (e.g., cell or tissue) and thereby allows a higher detection efficiency and more accurate marker localization.

### 5. Tissue characterization by autofluorescence

The autofluorescence can be characteristic for a certain tissue and therefore be used, e.g., for tumor detection. Typically, Two-Photon Excitation (TPE) is combined with Non-Descanned Detection (NDD) for deep tissue imaging, as these

applications are generally more prevalent in tissues or organisms.

### 6. Characterization and quality control of new materials

New materials of interest can be new fluorescent labels or quantum dots, which are used in biological imaging as well as in materials sciences. The minor carrier lifetime in semiconductor materials is an important parameter for the performance of these materials, e.g., in solar cells, OLEDs or laser materials and is determined by FLIM.

## Technical Realization

Time-Correlated Single Photon Counting (TCSPC) is used to determine the fluorescence lifetime. In TCSPC, one measures the time between sample excitation by a pulsed laser and the arrival of the emitted photon at the detector<sup>[1], [2]</sup>. TCSPC requires a defined “start” signal, provided by the electronics steering the laser pulse or a photodiode, and a defined “stop” signal, realized by detection with single-photon sensitive detectors (e.g., Single Photon Avalanche Diodes, SPADs). The measurement of this time delay is repeated many times to account for the statistical nature of fluorophore emission. The delay times are sorted into a histogram that plots the occurrence of emission over time after the excitation pulse.

In order to acquire a fluorescence lifetime image, the photons have to be attributed to the different pixels, which is done by storing the absolute arrival times of the photons additionally to the relative arrival time in respect to the laser pulse. Line and frame marker signals from the scanner of the confocal microscope are additionally recorded in order to sort the time stream of photons into the different pixels. A more detailed description of this so-called Time-Tagged Time-Resolved data mode as well as a detailed description of TCSPC can be downloaded from PicoQuant’s website<sup>[3]</sup>.

From a practical point of view, the integration of TCSPC requires the following hardware parts<sup>[4]</sup>:

#### 1. Pulsed light sources, for example:

- A picosecond pulsed laser of the desired excitation wavelength. Pulsed laser diodes (e.g., the LDH Series) have the advantage, that the laser repetition rate is adaptable to the lifetime of the dye through the laser driver (e.g., PDL 828 “Sepia II”).
- A pulsed femtosecond laser (usually a Ti:Sa laser) as used in TPE. These lasers are typically operated at a fixed repetition rate of 80 MHz.

Any laser used should provide a stable trigger output (SYNC) as a reference for the electronics. Otherwise, a fraction of the laser beam has to be guided onto a fast photodiode in order to generate a reference signal for the timing of the laser pulse.

2. Appropriate microscopic optics.  
Currently, confocal microscopes from all major microscope manufacturers can be upgraded, e.g.,
  - Leica SP2, SP5, and SP8
  - Nikon C1, C1si, C2, C2+, and A1
  - Olympus FluoView FV300, and FV1000
  - Zeiss LSM510, LSM710, and LSM780

The exact upgrading options depend on the system configuration. Apart from systems with beam scanning optics, also a piezo stage can be used

for sample or objective scanning, as realized in the MicroTime 200.

3. Single photon detection modules with appropriate sensitivity and time resolution.  
Detectors for FLIM imaging can be photomultiplier tubes (e.g., the PMA series), afterpulsing-free hybrid detectors (e.g., PMA Hybrid 40) or avalanche photodiodes (e.g., the PDM module from Micro Photon Devices or the PicoQuant's  $\tau$ -SPAD). Hybrid detectors and Single Photon Avalanche Diodes (SPADs) are sufficiently sensitive even for fluorescence correlation measurements, where single molecule sensitivity is required. PMTs and Hybrid detectors can furthermore be mounted in a NDD fashion for Two-Photon Microscopy applications.
4. Suited timing electronics for data registration (e.g., PicoHarp 300).

**Table 1: Environment sensitive dyes for sensing applications**

Dye	Application	References
Nitrobenzodiazole (NBD), Laurdan, di-4-ANEPPDHQ	Investigations on membrane structure and composition	[5], [6], [7]
MQAE, lucigenin-QDot nanosensor, Clomeleon	Cl <sup>-</sup> -concentration measurements in tissue	[8], [9], [10]
BCECF, Carboxy-(c-) SNAFL1, C-SNAFL2, fluorescein, C-fluorescein	pH measurements in living cells/tissue	[11], [12], [13]
Dextrimer compounds	Explosive sensing	[14]
Metall ligand complexes	Oxygen sensing	[15], [16]
NADH	Glucose sensing	[17], [18]
8-(alkoxy)-quinoline based probes	Protein content measurements	[19]
Rhodamine B, quantum dots	Temperature measurements	[20], [21]
Calmodulin, Mermaid, GcaMP2, di-8-ANEPPS, TN-XL, Calcium Green	Ca <sup>2+</sup> imaging	[22], [23], [24], [25]
“molecular beacon” or DNA-Hairpins	Specific DNA sequence detection	[26]
Amyloid FRET sensor	Amyloid formation	[27]
PreciSense Microsensor, FLIPglu-600 $\mu$ 13	Glucose monitoring	[28], [29]

- Data acquisition and analysis software to produce lifetime histograms, fit to different models, etc. (e.g., the SymPhoTime 64 software).

## FLIM Applications

### FLIM in sensing applications

FLIM is a valuable tool to assess changes of the molecular environment in the direct vicinity of fluorescently labeled molecules. Depending on the structure of the fluorophore, dyes can be sensitive to very different parameters. Examples are monitoring the concentration of Calcium ions ( $\text{Ca}^{2+}$ ), pH, oxygen, NADH or Chloride ( $\text{Cl}^-$ ).

An overview of different dyes and their use as sensors is provided in table 1. It shows only a selection and does not claim for completeness.

The sensitivity of a dye to a certain change of its local environment depends mainly on the dye structure, but sometimes also on the ambient conditions. For example, oxygen sensor dyes are usually quenched by collisional quenching with dissolved molecular oxygen. Given the solubility of oxygen in water and its diffusion coefficient, it is possible to calculate the quenching probability, which in this case is so low that fluorophores with lifetimes in the  $\mu\text{s}$  regime – usually metal complexes – have to be used.

Many specific sensors, e.g., for  $\text{Ca}^{2+}$ -determination are based on a construct that contains a donor/acceptor FRET pair. Binding to the target sample changes the internal conformation and thereby the FRET efficiency. These samples are discussed with some more detail in the section below dealing with intramolecular FRET changes.

Fig. 2 shows two applications demonstrating the

dependency of the fluorescence lifetime on the local environment. The label in the first example is the fluorescent dye Nitrobenzoxadiazole (NBD), that intercalates into lipid membranes and is quenched in the presence of water molecules (Fig. 2A). In contrast to lipid bilayers, micellar lipids allow access to water. Therefore, based on its different fluorescence lifetime, NBD is used to distinguish between micelles and lipid bilayers. An important biological sample, where this distinction improves our understanding, is the liver. This organ secretes bile fluids, that consist of micelle forming bile salts, phospholipids and cholesterol through hepatocytes into the canalicular space<sup>[30]</sup>. Measuring the fluorescence lifetime allows to localize bile fluids and distinguish them from the lipid bilayers of surrounding cell plasma membranes. The NBD labeled phospholipids were imaged in living hepatocytes originating from a cultivated cancer cell line (HepG2) which forms canalicular vacuoles.

The second example demonstrates  $\text{Cl}^-$ -sensing in cockroach salivary glands using the dye MQAE<sup>8</sup> (Fig. 2B and 2C). Cockroach glands are a well-established model system for studying epithelial ion transport. The fluorescence lifetime of the dye is quenched by  $\text{Cl}^-$ -ions, thus after calibration,  $\text{Cl}^-$ -concentration can be determined as well as the response time to various stimuli like different buffer concentrations wherein the salivary glands are embedded.

The two experiments were performed on different set-ups. Both samples have been analyzed with a MicroTime 200 microscope, but while NBD was excited with a pulsed diode laser, the  $\text{Cl}^-$ -concentration in the salivary glands was measured using a Ti:Sa laser system and TPE for deeper penetration into the tissue. Furthermore, this sample was scanned with a widerange scanner to map the complete gland.

### FLIM-FRET to detect molecular interactions

Förster Resonance Energy Transfer (FRET) has

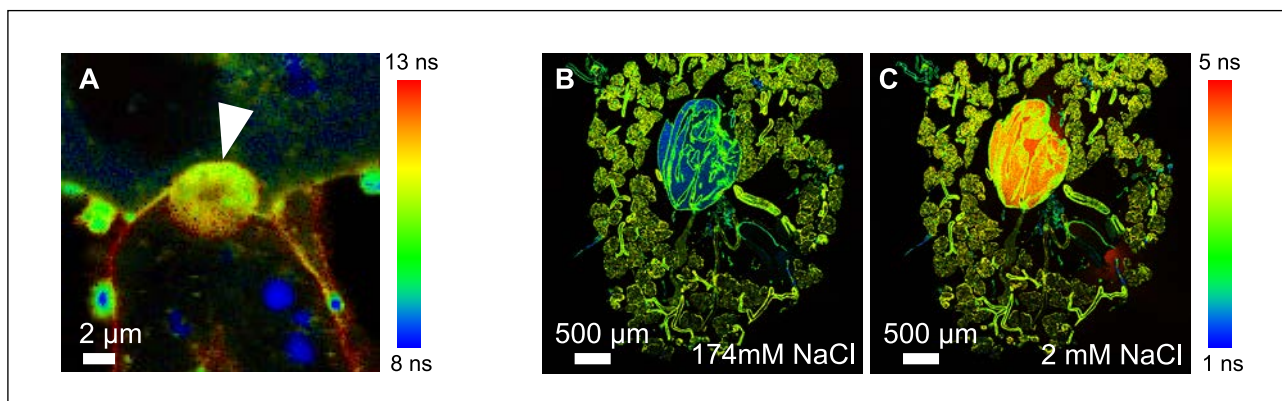


Fig. 2: Two examples for exploiting the fluorophore lifetime dependence on the local environment. A) Overview of HepG2 cells labeled with NBD tagged phospholipids. The vacuole (marked with the white arrowhead) is enriched with fluorescent phospholipids. The lifetime difference to other compartments is clearly visible and provides information about the membrane structure. B) and C) Dissected salivary glands of an American cockroach, labeled with MQAE and placed in buffers with 174 mM NaCl (B) and 2 mM NaCl (C). Courtesy of Carsten Hille, Carsten Dosche, Potsdam University, Germany.

become a valuable standard tool in cell biology to localize molecular interactions. In FRET, the phenomenon of energy transfer from the donor fluorophore to a suited acceptor molecule in close proximity results in excitation of the acceptor without acceptor-exciting laser light. FRET then causes a decrease in the donor emission and an increase in acceptor emission. Energy transfer can only occur when the donor emission and the acceptor excitation spectrum overlap and donor and acceptor fluorophore are in close proximity, usually less than 10 nm. Therefore, FRET is a tool to assess molecular interactions. However, quantification by intensity-based FRET is difficult since it bears the uncertainty of artifacts due to differences in excitation power, photo-bleaching or spectral crosstalk as well as the unknown concentrations of both molecules in living cells. Because the donor lifetime  $\tau_{DA}$  decreases in the presence of FRET, where the acceptor is the quenching molecule, FLIM offers a solution for quantitative analysis of molecular interactions and requires as control only measuring the fluorescence lifetime  $\tau_D$  of a donor-only labeled sample. The FRET efficiency  $E$  can then be easily calculated:

$$E = 1 - \frac{\tau_{DA}}{\tau_D} \quad (1)$$

If the donor decays more-exponentially, only an average FRET-efficiency can be calculated from the average lifetimes of the dye in a sample transfected with donor plus acceptor and a sample transfected with the donor only:

$$E_{average} = 1 - \frac{\tau_{DA+D, average}}{\tau_{D, average}} \quad (2)$$

If several molecules form a complex, intensity-based FRET is unable to distinguish if energy is transferred from all donor molecules with low FRET efficiency (e.g., due to distances larger than the Förster radius) or if only a few donor molecules are tightly bound in the complex enabling high efficiency of energy transfer between donor and acceptor.

As the lifetime measurement is able to resolve a multiple exponential decay, FLIM-FRET can distinguish between these two situations, if the fluorescence decay behavior of the donor alone can be described by a mono-exponential decay. In this case, an overall low FRET efficiency results in a single exponential decay, whereas in case of high FRET efficiency between only a few molecules, a multi-exponential fitting model must be applied to determine the fluorescence lifetime. In a system where reversible binding occurs, the shorter lifetime component corresponds then to the lifetime of the donor in presence of the acceptor  $\tau_{DA}$ , while the longer lifetime should equal

the time of the donor in the absence of the acceptor  $\tau_D$ . As in FRET systems, the fractional amplitudes fitted as in Eq. 3 equal the fractional concentrations, the amount of the bound population can be calculated directly from the amplitudes (Eq. 4).

$$\tau_{average} = \frac{\sum_i A_i \tau_i}{\sum_i A_i} \quad (3)$$

$$\frac{c_{DA}}{c_{DA} + C_D} = \frac{A_{DA}}{A_{DA} + A_D} \quad (4)$$

It is important to stress that this calculation as in Eq. 4 is only possible for donor dyes with a single exponential decay behavior. Several examples for such fluorescent proteins have been published, e.g.,

- mTurquoise, mTurquoise 2<sup>[31], [32]</sup>
- mTFP1<sup>[33]</sup>
- T-Sapphire<sup>[34]</sup>
- Citrine<sup>[35], [36]</sup>, pH-dependent
- EYFP<sup>[37], [38]</sup>
- TagRFP<sup>[39]</sup>

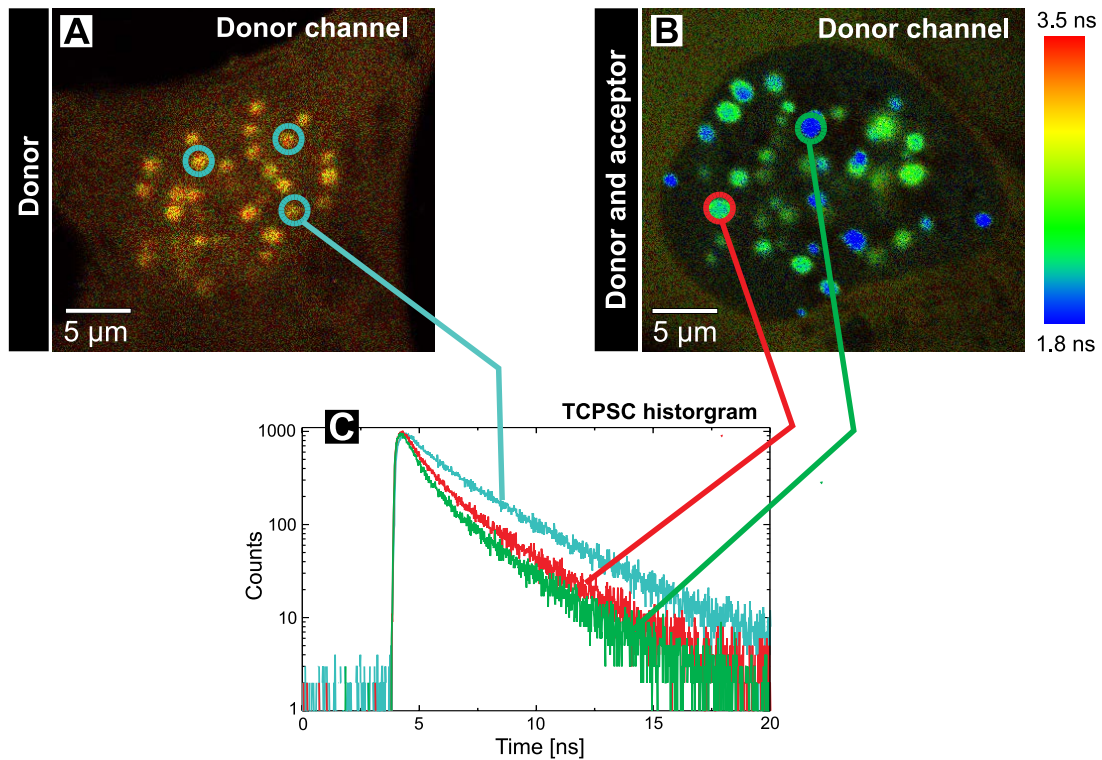
The following example demonstrates the use of FLIM-FRET in cell applications.

The human centromere kinetochore complex is responsible for correct chromosome segregation during cell division. This complex consists of about 50 kinetochore proteins (CENPs) and the underlying DNA structure – the centromere. Malfunction of this complex can lead to aneuploidy and cancer<sup>[40], [41]</sup>. Although many components of this essential complex are known, its exact structure still remains unsolved. Therefore, the neighborhood relations of kinetochore proteins were determined in living human cells by FLIM-FRET.

Fig. 3 displays a FLIM-FRET experiment with the two kinetochore proteins CENP-A and -B. CENP-B and CENP-A have been tagged with the fluorophores Cerulean and EYFP at their C- and N-terminus respectively and display a punctual localization at centromeres in the cell nucleus. The measurements were performed in transiently transfected living human cells.

Fig. 3A shows FLIM on control cells expressing only the donor Cerulean fused to CENP-B. Calculation of the lifetimes of three centromeres (marked with blue circles) showed an average donor lifetime of 3 ns (Fig. 3A and the blue trace in Fig. 3C). In a cell containing both donor CENP-B-Cerulean and accep-

### Single channel detection



### Dual channel detection

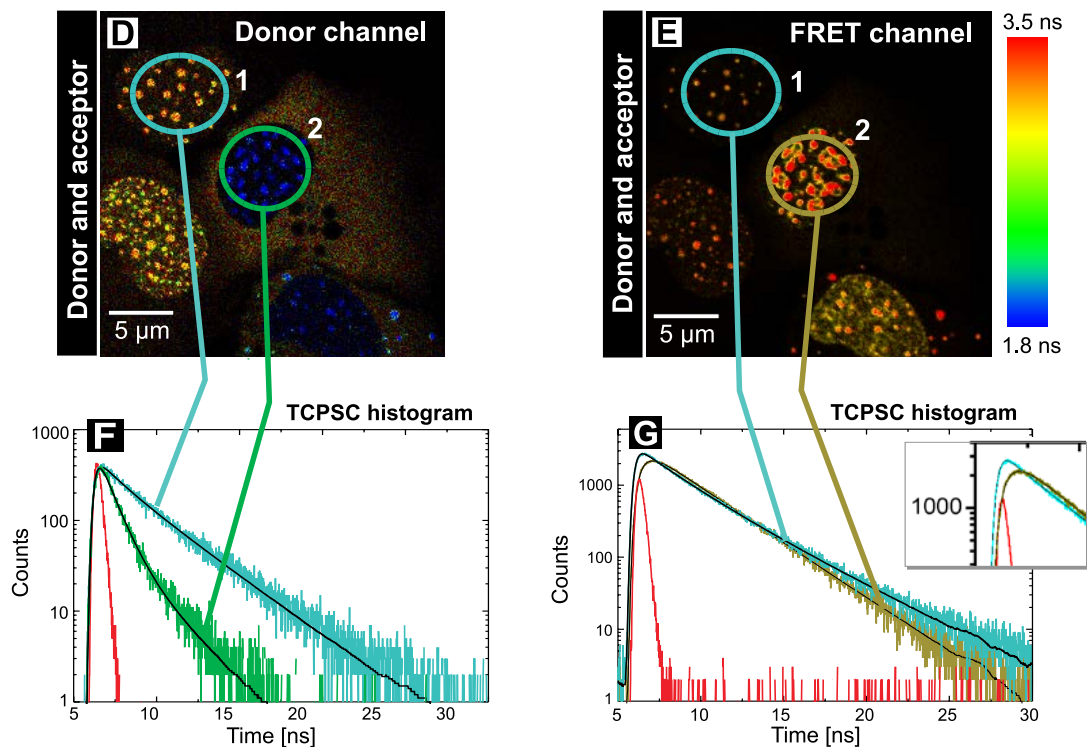


Fig. 3: FLIM-FRET measurements of the human kinetochore proteins CENP-A and CENP-B. FLIM images of human U2OS cells transfected with the donor CENP-B-Cerulean (A) or additionally with the acceptor EYFP-CENP-A (B) display the donor fluorescence lifetime (single channel detection). The blue decay curve in the TCSPC histogram (C) corresponds to the three blue-circled centromeres of the control cell (A), whereas the green and red lines represent fluorescence decays of the indicated centromeres in the FRET cell (B). The fluorescence lifetime is indicated by a false color representation. Analysis of a single tagged cell (cell 1) and a double tagged FRET cell (cell 2) with indicated lifetime histograms in the donor (D and F) and acceptor channel (E and G).

tor EYFP-CENP-A (Fig. 3B), the average donor lifetime was decreased. At two single centromeres the average fluorescence lifetimes were shifted towards 1.8 ns and 2.2 ns, respectively (green and red circles and traces in Fig. 3B and C, respectively). Thus, one can conclude that both proteins are in direct vicinity in human kinetochores.

For this analysis, the fluorescence lifetimes were calculated by fitting the fluorescence decay to a bi-exponential model. Whereas the control cell showed a homogeneous and longer average lifetime in all centromeres, in the double transfected FRET cell the fluorescence lifetimes of the different centromeres is clearly shortened. With these experiments it could be demonstrated that both the N-terminus of CENP-A and the C-terminus of CENP-B are in very close vicinity in the kinetochore complex.

To complete the picture, the technique of using two channel FLIM is helpful for the analysis of heterogeneous samples, like living cells with exogenous protein expression. In this way, the FRET channel serves as an additional control to demonstrate the presence of the acceptor dye. Dual channel FLIM-FRET was performed using two detectors to monitor the fluorescence lifetime of both the donor (Fig. 3D) and acceptor fluorophores simultaneously after excitation of the donor at 440 nm (Fig. 3E). Channel one displays the donor lifetime whereas in the second channel the acceptor fluorescence decay is shown.

Cell 1 in Fig. 3D/3F marked with a blue circle contained only the donor CENP-B-Cerulean. The weak fluorescence seen in the acceptor channel was caused by bleed through and the measured lifetime in the acceptor channel matches the lifetime meas-

ured in the donor channel (cell marked in blue in Fig. 3D/3E and corresponding decay curves).

In cell 2, both donor and acceptor molecules were present. In the donor channel, the quenching of the lifetime down to 1.2 ns caused by FRET is indicated by the blue color of all centromeres. A FRET efficiency of 60% was calculated. In the FRET channel, strong fluorescence of the acceptor EYFP-CENP-A was detected. The decay time in the acceptor channel of 2.8 ns for this cell corresponds to the acceptor EYFP (dark green trace in Fig. 3G). In addition, a rise time of around 0.5 ns was observed (see enlargement in the TCSPC histogram). This delay of acceptor emission was caused by energy transfer between the donor and acceptor. A coordinated analysis of the donor and acceptor decay has been proposed by Laptenok et al.<sup>[42]</sup>.

### Conformational changes in FLIM

While in intracellular FLIM measurements using two constructs labeled with donor and acceptor fluorophores, the exact concentration of both dyes is not known, in conformational studies macromolecules of interest are labeled with both donor and acceptor dyes. Therefore, the donor/acceptor stoichiometry in these samples is fixed. In order to study conformational changes of a macromolecule, measurements on the single molecule level are crucial in order to resolve subpopulations and the rates of conformational dynamics (Fig. 4).

On the one hand, conformational changes are interesting as a topic to study by itself, e.g., folding dynamics<sup>[43], [44], [45]</sup>, but more frequently, specially designed double labeled macromolecules are used

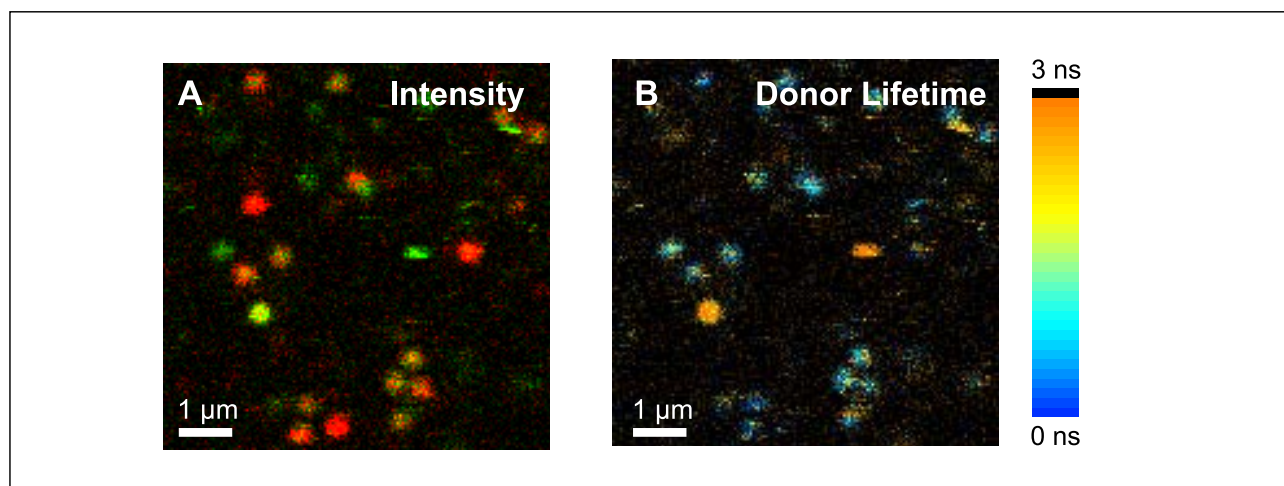


Fig. 4: Intramolecular FRET to monitor conformational changes. An RNA oligonucleotide with a tetraloop receptor sequence was labeled with a FRET pair (Cy3/Cy5). Conformational changes which are heavily influenced by  $Mg^{2+}$ -binding have been monitored. The image shows individual, double-labeled RNA molecules in a buffer solution with 1 mM  $Mg^{2+}$ , where both conformations (open = no FRET and closed = FRET) are present<sup>43</sup>. A) Dual-channel intensity image of individual immobilized tetraloop receptor RNAs upon donor and acceptor excitation. The Cy3 (donor) intensity is shown in green, while the Cy5 (acceptor) intensity is indicated in red. Molecules labeled with both dyes appear in yellow or orange, depending on the FRET efficiency. B) Fluorescence lifetime image of the donor CY3. The different lifetimes can be attributed to different conformations of the RNA, depending on the  $Mg^{2+}$ -binding. Courtesy of Julie Fiore, David Nesbitt, University of Colorado, USA.

as sensor samples.

From a mechanistic point of view, mainly FRET sensors are used, but also electron transfer is a suitable quenching mechanism and even more sensitive to conformational changes. Many dyes are quenched by the DNA base guanosin, which can be exploited in DNA hairpin sensors. They become unquenched when the probe binds to a DNA with a complementary sequence<sup>[26]</sup>. In protein studies, mainly tryptophan is known as an effective quencher which allows for analysis of protein dynamics<sup>[46]</sup>.

From a structural point of view, sensors can be designed including either chemical dyes or genetically encoded fluorescent proteins (e.g., EGFP and its derivatives). Especially fluorescent proteins are widely-used, as often only their expression allows efficient and mild labeling of living cells. However, the maturing of the distinct fluorescent proteins have to be considered in these applications.

As the chromophoric group of fluorescent proteins is relatively well shielded, sensors including such fluorescent proteins are commonly based on the FRET mechanism. Many of the sensors listed in table 1 work on this principle and change their conformation upon binding of another molecule, e.g., Calmodulin or Mermaid. Both alter their structure upon binding to Calcium ions, which is applied to study neuron behavior. Thus, with such sensors, the exact concentration of a certain ligand can be determined.

Furthermore, proteins of interest are modified to study structural changes upon ligand binding, as, e.g., done in the case of a FRET based sensor fused to the adapter protein CrkII, where phosphorylation processes at this protein were studied<sup>[47]</sup>. In a similar fashion, many proteins could be analyzed using this approach. And finally, stress sensitive sensors have been developed to monitor mechanical force on the cytoskeleton<sup>[48]</sup>.

## Discrimination of multiple fluorescent labels and background removal

The simplest approach to distinguish different fluorescent signals in biological specimen is the discrimination of an introduced label from autofluorescence. This application is especially important in tissue samples and plant cells. In labeled cells with an autofluorescent environment, this additional information provided by the fluorescence lifetime can be used in order to separate a fluorescent label from the autofluorescent background<sup>[49]</sup>. (Fig. 5).

On the other hand, due to the increasing number of fluorescent proteins and specific labeling techniques, it has become possible to stain multiple target molecules in parallel and observe their interactions as well as their multiple localizations within the sample. This rises the question about how to discriminate between the various labels. In the classical way using a spectral approach, the multiple components in such a system are stained each with spectrally different fluorophores allowing for multicolor imaging<sup>[50]</sup>.<sup>[51]</sup>.<sup>[52]</sup> Spectral unmixing helps to raise the number of distinguishable labels. This number is even increased by including the fluorescence lifetime as an additional parameter. Consequently, more fluorophores can be monitored and separated simultaneously within a sample.

## Autofluorescence FLIM for tissue discrimination

Autofluorescence provides highly specific information about certain tissues and is therefore commonly used in medical oriented applications. Often, Two-Photon Excitation (TPE) is applied for several reasons:

- The penetration depth for longer wavelengths as used in TPE is larger, therefore, thicker tissue samples can be imaged.
- The excitation spectra for TPE are often broader compared to visible light. Consequently, more dif-

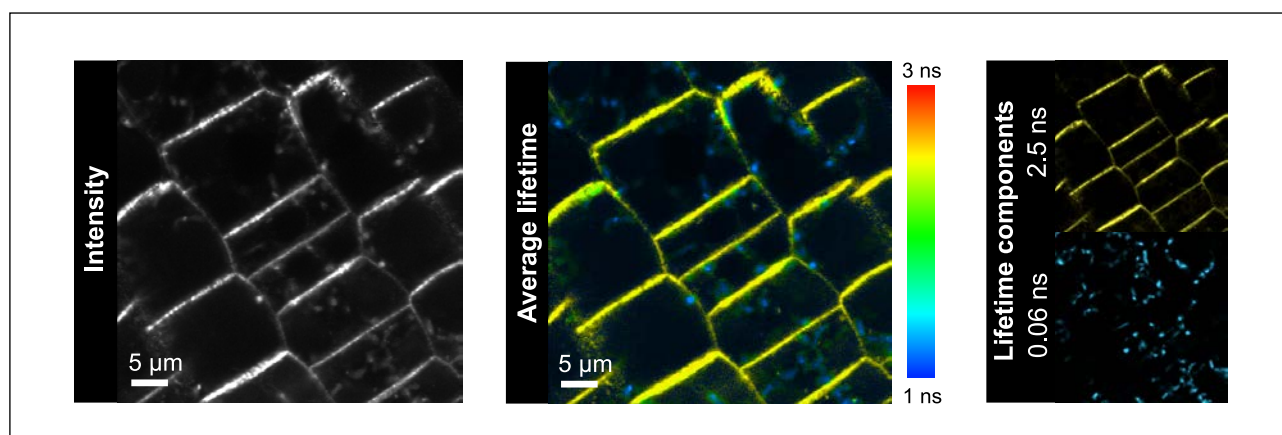


Fig. 5: Discrimination of autofluorescence from a fluorescent label. This example from plant biology shows *Arabidopsis* root cells transformed with a GFP-tagged PIN2 variant. The PIN-protein group is involved in root gravitology. PIN2-GFP excited with a pulsed 470 nm laser has a significant longer lifetime than the autofluorescence of the *Arabidopsis* root cells. A three-component lifetime fit was applied and the 2.5 ns component was specific for GFP fluorescence. Courtesy of Alexander Dovzhenko, Klaus Palme, Freiburg University, Germany.

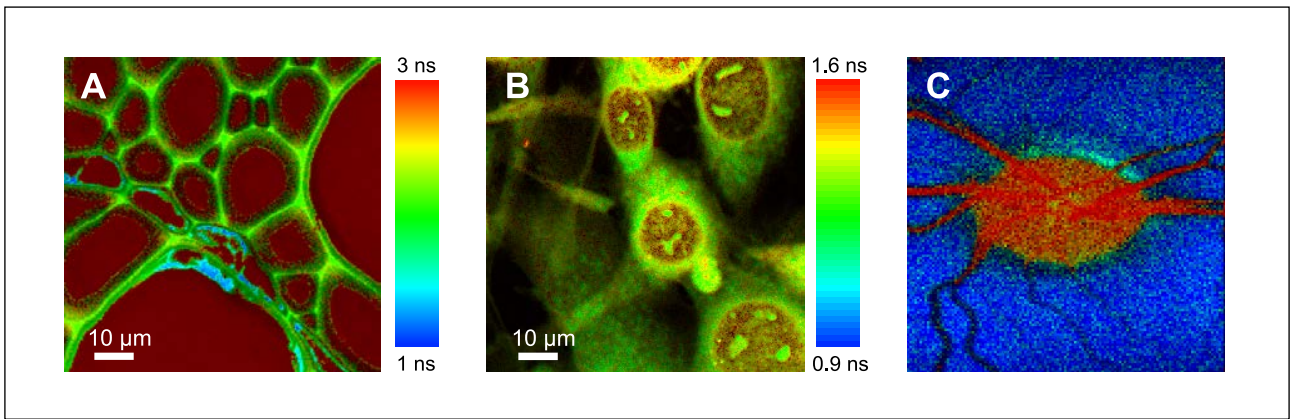


Fig. 6: Examples for autofluorescence imaging: A) Unstained lime tree sample excited with a fs-pulsed laser at 1030 nm. The FLIM image of the autofluorescence upon TPE shows strong contrast in the different morphological parts of the sample. B) Native fluorescence of 3T3 cells measured on an UV-optics adapted MicroTime 200 and excited with a pulsed 266 nm laser based on a Master Oscillator Fiber Amplifier (MOFA) with added frequency conversion. C) Fluorescence Lifetime Image of the retina showing the optical nerve in the center. Courtesy of Prof. Schweitzer, Ophthalmic Hospital at the University of Jena, Germany

ferent fluorophores are excited and potentially a larger image contrast can be obtained.

A distinct autofluorescent compound that was targeted already in early days of fluorescence lifetime imaging is nicotinamid-adenin-dinucleotide (NADH)<sup>[53]</sup>, as bound and unbound NADH show huge differences in their lifetime (protein-bound NADH ~2 ns, free NADH ~0.3 ns<sup>[54]</sup>).

Autofluorescence decays are often complex, thus the primary aim of these investigations is the detection of specific differences between tissues. This comparison then allows, e.g., to discriminate between healthy and carious dental tissue<sup>[55]</sup>, arteriosclerotic plaques<sup>[56], [57]</sup> and to identify sub-structures within the retina<sup>[58]</sup> and skin<sup>[59]</sup> (Fig. 6).

### FLIM in materials sciences

Applications in materials science are mainly focused on the fundamental characterization of new materi-

als<sup>[60], [61]</sup> as used, e.g., in photovoltaics<sup>[62], [63], [64], [65]</sup>, OLEDs<sup>[66]</sup>, light harvesting materials<sup>[67], [68], [69]</sup> and functionalized surfaces<sup>[70], [71]</sup>.

As often inorganic materials are subject to investigation, lifetime measurements are usually called Time-Resolved Photoluminescence (TRPL) studies. (Fig. 7). An important material in this research field are quantum or nano-dots and other types of nano-materials that are used in a broad range of applications as dye sensitized solar cells, photodynamic therapy or labels in biological sciences<sup>[72], [73], [74]</sup>.

In investigations on semiconductors, the minor carrier lifetime is observed. Here, the luminescence is caused by transitions between the conduction and the valence band. As charges in the conduction band as well as holes in the valence band are mobile, recombination rates usually depend on the excitation intensities and the size of the excitation volume in case of confocal microscopy. But of more interest is

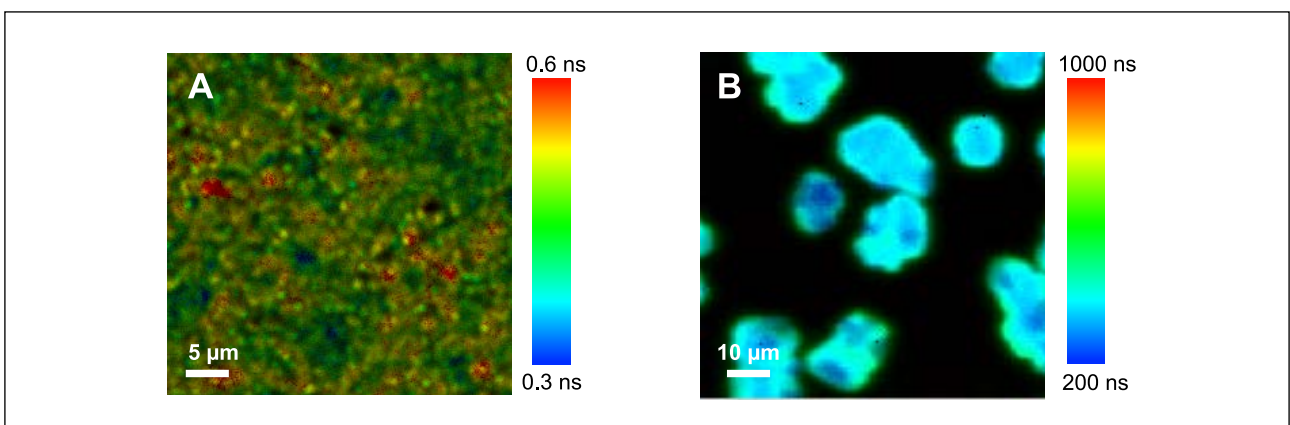


Fig. 7: Fast and slow kinetics of different materials. A) Time Resolved Photoluminescence (TRPL) image of a CdTe thin film device. The sample was excited with 635 nm and detected around 850 nm using a  $\tau$ -SPAD detector. A typical grain-like structure as well as sub-structures with different minor carrier lifetimes are clearly visible. Courtesy of Christian Kraft, University of Jena, Germany. B) Luminescence image of Tris(bipyridine)ruthenium(II) dichloride (RuBiPy)-crystals excited at 375 nm. The luminescence lifetime is in the range of a few hundred ns and crystals are not completely uniform, which may be explained with different crystallization or oxygen accessibility.

the fact that the minor carrier lifetime is very much influenced by impurities, which can constitute traps for minor carriers, or – in case of thin film devices – by the quality of the surface passivation. This makes the minor carrier lifetime an important parameter to control or improve the quality of a fabrication procedure. For lifetime measurement possibilities in semiconductor materials, a dedicated application note can be downloaded<sup>[75]</sup>.

## Conclusion and Outlook

Fluorescence lifetime imaging microscopy enables addressing questions in very different fields of research, and up to now, several thousand papers dealing with fluorescence lifetime measurements have been published. Time-Correlated Single Photon Counting (TCSPC) is a key method in this field with a sensitivity allowing for fluorescence lifetime measurements down to the single molecule level. In the future, a combination of lifetime measurements with spectral or dynamic information opens promising prospects, e.g., in Calcium imaging or multi label discrimination<sup>[23], [76]</sup>.

Another approach combines topological information provided by an AFM with lifetime information. Previously, acquisition of topographic information and

molecular behavior as detected by FLIM was limited to correlative experiments, requiring large amounts of statistics especially for heterogeneous biological samples. With a combined FLIM AFM set-up, as realized in the MicroTime 200 microscope with a mounted AFM, already the data are acquired in a simultaneous and correlated fashion.

In Fig. 8, fixed glioblastoma cells (brain cancer cells) were investigated simultaneously with AFM and fluorescence microscopy (Sample Courtesy of Celine Heu, FEMTO, Besancon, France). The cells expressed a freely diffusible Green Fluorescent Protein (GFP). All images visualize the investigated cells whereas each image contains a different fluorescence or nanomechanical information. In Fig. 8A and 8E, the intensity modulated GFP lifetime and localization in the cells are shown, respectively. The free GFP localizes to all parts of the cells with accumulation in the nucleus. As expected, no changes in lifetime were detected. Fig. 8B-8H shows the information taken by the BioScope Catalyst (Bruker AXS, Madison, WI, USA) in PeakForce QNM mode. By measuring and analyzing a force curve at every image point, one obtains topography, modulus, adhesion, deformation and dissipation of the cell. The measurement was made quantitatively by prior spring constant calibration of the AFM cantilever using the integrated thermal-noise calibration method. The fluorescence intensity (photon counts) was recorded

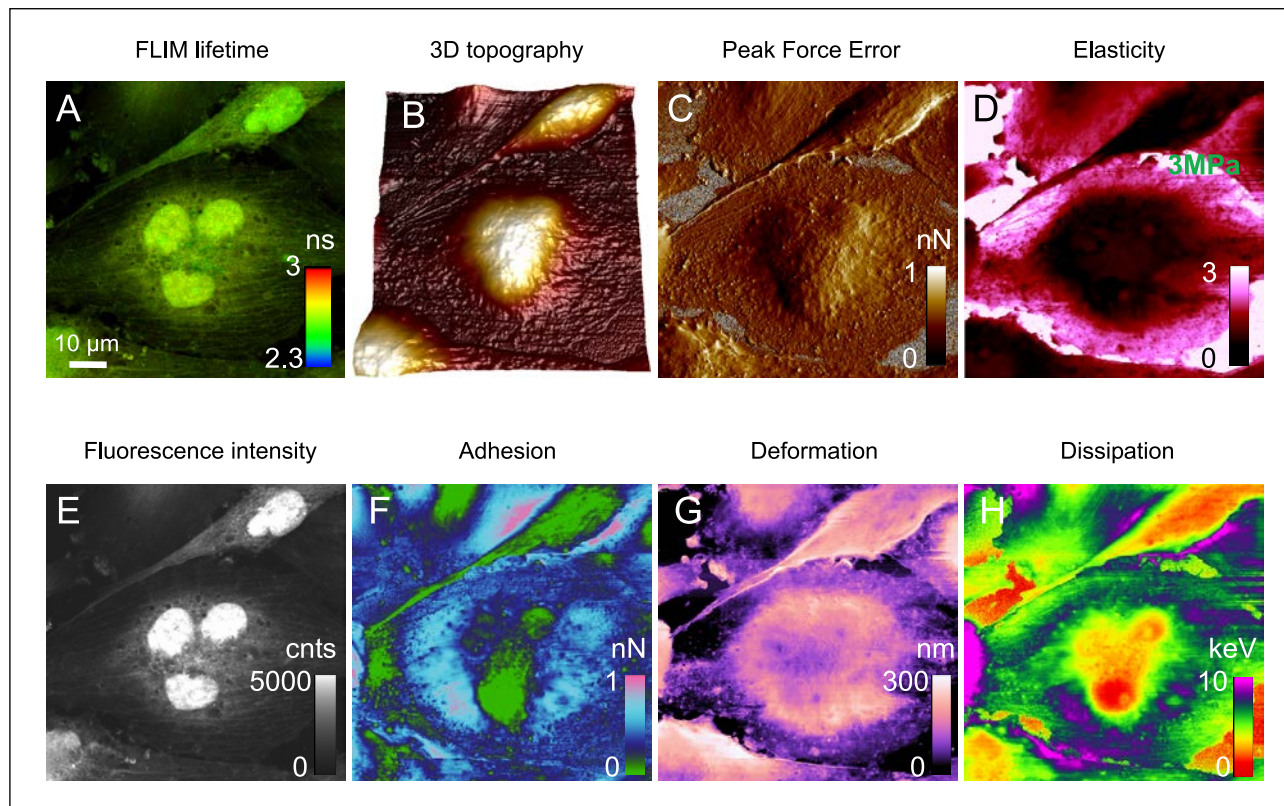


*Fig. 8: Synchronized acquisition of fixed glioblastoma cells expressing GFP using the MicroTime 200 in combination with the BioScope Catalyst (Bruker, Madison, WI, USA). (A) Fluorescence lifetime distribution in the cells, acquired by the MicroTime 200. (B-D,F-H) Data taken by the BioScope Catalyst AFM in PeakForce QNM mode, showing topography and spatially resolved quantitative mechanical cell properties. (E) Photon counts from MicroTime 200 are synchronously recorded by the Nanoscope AFM controller.*

pixel-synchronously with the AFM measurement by distributing the digital information from the single photon detector (SPCM-AQR-14 SPAD, Perkin Elmer) into the Nanoscope-V AFM controller's pulse counting input. The overlay of the images from those two instruments was realized by exporting the FLIM image and overlaying it in Bruker's MIRO software. The data were acquired in collaboration with Bruker Corporation.

Currently, AFMs from three companies can be combined with PicoQuant's MicroTime 200:

- BioScope Catalyst from Bruker AXS, Madison, WI, USA
- MFP-3D BIO from Asylum Research, Santa Barbara, CA, USA
- NanoWizard3 from JPK Instruments, Berlin, Germany<sup>[77]</sup>

The increasing interest in lifetime techniques will trigger new fields of applications, new analysis schemes as well as improvements in the labels, e.g., by developing new single exponentially decaying fluorescent proteins covering a broad spectral range.

## References

- [1] M. Wahl, Time-Correlated Single Photon Counting. Technical Note, [http://www.picoquant.com/technotes/technote\\_tcspc.pdf](http://www.picoquant.com/technotes/technote_tcspc.pdf) (2009)
- [2] J. R. Lakowicz, Principles of Fluorescence Spectroscopy, 3rd Edition, Springer
- [3] M. Wahl, Time-tagged Time-resolved Data collection. Technical Note, (2004)
- [4] B. Krämer, V. Buschmann, U. Ortmann, M. Wahl, A. Bülter, F. Koberling, R. Erdmann, Compact FLIM and FCS Upgrade Kit for Laser Scanning Microscopes (LSMs). Technical Note, (2012)
- [5] A. Bunge, M. Fischlechner, M. Loew, A. Arbutova, A. Hermann, D. Huster, Characterization of lipid bilayers adsorbed on spherical LbL-support. *Soft Matter*, 5, 3331-3339 (2009)
- [6] M. Stöckl, A. P. Plazzo, T. Korte, A. Herrmann, Detection of lipid domains in model and cell membranes by fluorescence lifetime imaging microscopy of fluorescent lipid analogues. *J. Biol. Chem.*, 283, 30828-30837 (2008)
- [7] D. M. Owen, K. Gaus, Optimized Time-Gated Generalized Polarization Imaging of Laurdan and di-4-ANEPPDHQ for Membrane Order Image Contrast Enhancement, *Micr. Res. and Tech.*, 73, 618-622 (2010)
- [8] M. Lahn, C. Drosche, C. Hille, Two-photon microscopy and fluorescence lifetime imaging reveal stimulus induced intracellular Na<sup>+</sup> and Cl<sup>-</sup> changes in cockroach salivary acinar cells. *Am J Physiol Cell Physiol*, 300(6), 1323-1236 (2011)
- [9] M.J. Ruedas-Rama, A. Orte, E. A. H. Hall, J. M. Alvarez-Pez, E. M. Talavera, A chloride ion nanosensor for time-resolved fluorimetry and fluorescence lifetime imaging, *Analyst*, 137, 1500-1508 (2012)
- [10] M. Jose, D. K. Nair, C. Reissner, R. Hartig, W. Zuschratter, Photophysics of clomeleon by FLIM: Discriminating Excited State Reactions along Neuronal Development, *Biophys. J.*, 92, 2237-2254 (2007)
- [11] C. Hille, M. Berg, L. Bressel, D. Munzke, P. Primus, H.-G. Löhmannsröben, C. Dosche, Time-domain fluorescence lifetime imaging for intracellular pH sensing in living tissues, *Anal. Bioanal. Chem.*, 391, 1871-1879 (2008)
- [12] R. Sander, A. Draaijer, H.C. Gerritsen, P.M. Hout, Y.K. Levine, Quantitative pH imaging in cells using confocal fluorescence lifetime microscopy. *Anal. Biochem*, 227(2), 302-308 (1995)
- [13] H. J. Lin, P. Herman, J. R. Lakowicz, Fluorescence lifetime-resolved pH imaging of living cells. *Cytometry*, 52(2), 77-89 (2003)
- [14] D. A. Olley, E.J. Wren, G. Vamvounis, M. J. Fernee, X. Wang, P. L. Burn, P. Meredith, P. E. Shaw, Explosive Sensing with Fluorescent Dendrimers: The Role of Collisional Quenching, *Chem. of Materials*, 23, 0789-0794 (2011)
- [15] J. Lopez-Gejo, D. Haigh, G. Orellana, Relationship between the Microscopic and Macroscopic World in Optical Sensing: A Luminescence Lifetime Study, *Langmuir*, 26(3), 2144-2150 (2010)
- [16] D. Sud, M. A. Mycek, Calibration and validation of an optical sensor for intracellular oxygen measurements. *JBO*, 14(2), 020506(1)-020506(3) (2009)
- [17] A. von Ketteler, D. Sieberg, D.-P. Herten, C. Horn, W. Petrich, Fluorescence Lifetime-Based Glucose Sensing using NADH, *Proc. SPIE*, 8229, 82290P-1 (2012)
- [18] D. Sud, W. Zhong, D. G. Beer, M. A. Mycek, Time-resolved optical imaging provides a molecular snapshot of altered metabolic function in living human cancer cell models. *Opt Express*, 14, 4412-4426 (2006)
- [19] B. Olha, G. Das, Environment-sensitive amphiphilic fluorophore for selective sensing of protein, *Photochem. & Photobiol. Stud.*, 10, 554-560 (2011)
- [20] M. A. Bennet, P.R. Richardson, J. Arlt, A. McCarthy, G. S. Buller, A. C. Jones, Optically trapped microsensors for microfluidic temperature measurement by fluorescence lifetime imaging microscopy, *Lab Chip*, 11, 3821-3828 (2011)
- [21] T. Fujii, Y. Taguchi, T. Saiki, Y. Nagasaka, A Fusion Near-Field Optical Fiber Probe Using Photonic Crystal Fiber for Nanoscale Thermometry Based on Fluorescence-Lifetime Measurement of Quantum Dots, *Sensors*, 11(9), 8358-8369 (2011)
- [22] A. Miyawaki, J. Llopis, R. Heim, J. M. McCaffery, J. A. Adams, Fluorescent indicators for Ca<sup>2+</sup> based on green fluorescent proteins and calmodulin. *Nature* 388: 882-887 (1997)
- [23] Q. Tian, M. Oberhofer, S. Ruppenthal, A. Schloz, V. Buschmann, H. tsuitsui, A. Miyawaki, A. Zeug, P. Lipp, L. Kaestner, Optical action potential screening on adult ventricular myocytes as an alternative QT-screen, *Cellular Physiol. and Biochem.*, 27, 281-290 (2011)
- [24] M. Mank, D. F. Reiff, N. Heim, M. W. Friedrich, A. Borst, O. Griesbeck, A FRET-based calcium biosensor with fast signal kinetics and high fluorescence change, *Biophys. J.*, 90(5), 1790-1796 (2005)
- [25] A. Celli, S. Sanchez, M. Behne, T. Hazlett, E. Gratton, T. Mauro, The epidermal Ca(2+) gradient: Measurement using the phasor representation of fluorescent lifetime imaging. *Biophys J.*, 98(5): 911-921 (2010)
- [26] O. Piester, H. Barsch, K. Weston, V. Buschmann, T. Heinlein, J. P. Knemeyer, K. D. Weston, M. Sauer, A Single-Molecule DNA Hairpin System Based on Intramolecular Electron Transfer, *Nano Letters*, 3(7), 979-982 (2003)
- [27] G. S. Kaminski Schierle, C. W. Bertoncini, F. T. Chan, A. T. Van der Goot, S. Schwendler, J. Skepper, S. Schlachter, T. van Ham, A. Esposito, J. R. Kumita, E. A. Nollen, C. M. Dobson, C. F. Kaminski, A FRET sensor for non-invasive imaging of amyloid formation in vivo, *Chemphyschem*, 12(3), 673-680 (2011)
- [28] J. K. Nielsen, J. S. Christiansen, J. S. Kristensen, H. O. Toft, L. Lundby Sanden, S. Aasmul, K. Gregorius, Clinical Evaluation of a Transcutaneous Interrogated Fluorescence Lifetime-Based Microsensor for Continuous Glucose Reading, *J Diabetes Sci Technol.*, 3(1), 98-109 (2009)
- [29] H. Takanaga, B. Chaudhuri, W. B. Frommer, GLUT1 and GLUT9 as the major contributors to glucose influx in HEPG2 cells identified by a high sensitivity intramolecular FRET sensor, *Biochim Biophys Acta*, 1778(4), 1091-1099 (2008)

- [30] A. Tannert, D. Wüstner, J. Bechstein, P. Müller, P. F. Devaux, A. Herrmann, Aminophospholipids have no access to the luminal side of the biliary canaliculus: implications for the specific lipid composition of the bile fluid, *J Biol Chem.*, 278 (42):40631-40639 (2003)
- [31] J. Goedhart, L. van Weeren, M. A. Hink, N. O. E. Vischer, K. Jalink, T. W. J. Gadella, Bright cyan fluorescent protein variants identified by fluorescence lifetime screening, *Nature Methods*, 7(2), 137-139 (2010)
- [32] J. Goedhart, D. von Stetten, M. Noirclerc-Savoie, M. Lelimosin, L. Joosen, M. A. Hink, L. van Weeren, T. W. J. Gadella, A. Royant, Structure-guided evolution of cyan fluorescent proteins towards a quantum yield of 93%, *Nature Communications*, 3, 751 (2012)
- [33] H. Ai, J. N. Henderson, S. J. Remington, R. E. Campbell, Directed evolution of a monomeric, bright and photostable version of *Clavularia cyan fluorescent protein*: structural characterization and applications in fluorescence imaging, *Biochem. J.*, 400, 531-540 (2006)
- [34] V. Bayle, L. Nussaume, R. A. Bhat, Combination of Novel Green Fluorescent Protein Mutant Tsapphire and DsRed Variant mOrange to Set Up a Versatile in Planta FRET-FLIM Assay, *Plant Physiology*, 148, 51-61 (2008)
- [35] B. G. Abraham, N. V. Tkachenko, V. Santala, H. Lemmetyinen, M. Karp, Bidirectional Fluorescence Resonance Energy Transfer (FRET) in Mutated and Chemically Modified Yellow Fluorescent Protein (YFP), *Bioconj. Chem.*, 22,227-234 (2011)
- [36] A. A. Heikal, S.T. Hess, G. S. Baird, R.Y. Tsien, W. W. Webb, Molecular spectroscopy and dynamics of intrinsically fluorescent proteins: coral red (dsRed) and yellow (Citrine). *PNAS*, 97(22), 11996-12001 (2000)
- [37] O. Rocks, A. Peyker, M. Kahms, P.J. Verveer, C. Koerner, M. Lumbierres, J. Kuhlmann, H. Waldmann, Ah. Wittinghofer, P.I.H. Bastiaens, An Acylation Cycle Regulates Localization and Activity of Palmitoylated Ras Isoforms, *Science* 307, 1746-1752 (2005)
- [38] A. Peyker, O. Rocks, P.I.H. Bastiaens, Imaging Activation of Two Ras Isoforms Simultaneously in a Single Cell, *ChemBioChem* 6, 78-85 (2005)
- [39] A. L. Rusanov, T. V. Ivashina, L.M. Vinokurov, I. I. Fiks, A. G. Orlova, I. V. Turchin, I. G. Meerovich, V. V. Zherdeva, A. P. Savitsky, Lifetime imaging of FRET between red fluorescent proteins, *J. Biophotonics*, 3(12), 774-783 (2010)
- [40] S. Orthaus, V. Buschmann, A. Bülter, S. Fore, M. König, R. Erdmann, Quantitative in vivo imaging of molecular distances using FLIM-FRET, Application Note, [http://www.picoquant.com/technotes/appnote\\_flim\\_fret.pdf](http://www.picoquant.com/technotes/appnote_flim_fret.pdf) (2009)
- [41] S. Orthaus, C. Biskup, B. Hoffmann, C. Hoischen, S. Ohndorf, K. Benndorf, S. Diekmann, Assembly of the Inner Kinetochore Proteins CENP-A and CENP-B in Living Human Cells, *ChemBioChem*, 9, 0077-0092 (2008)
- [42] S. P. Laptinok, J. W. Borst, K. M. Mullen, I. H. Van Stokkum, A.J. Visser, H. van Amerongen, Global analysis of Förster resonance energy transfer in live cells measured by fluorescence lifetime imaging microscopy exploiting the rise time of acceptor fluorescence, *Phys Chem Chem Phys*, 12(27), 7593-602 (2010)
- [43] B. Schuler, W. A. Eaton, Protein Folding studied by single-molecule FRET, *Curr. Opin. in Struct. Biol.* 18, 016-026 (2008)
- [44] H. K. Kim, I. Rasnik, J. Liu, T. Ha, Y. Lu, Dissecting metal ion-dependent folding and catalysis of single DNAzyme, *Nat Chem Biol*, 3(12), 763-768 (2007)
- [45] J. Fiore, B. Kraemer, F. Koberling, R. Erdmann, D. Nesbitt, Enthalpy-Driven RNA Folding: Single-Molecule Thermodynamics of Tetraloop Receptor Tertiary interaction, *Biochemistry*, 48(11), 2550-2558 (2009)
- [46] N. Marmé, J. P. Knemeyer, M. Sauer, J. Wolfrum, Inter- and Intramolecular Fluorescence Quenching of Organic Dyes by Tryptophan, *Bioconj. Chem.*, 14, 1133-11139 (2003)
- [47] K. Kurokawa, N. Mochizuki, Y. Ohba, H. Mizuno, A. Miyawaki, M. Matsuda, A pair of fluorescence energy transfer-based probes for tyrosine phosphorylation of the Crkl adaptor protein in vivo, *J. Biol. Chem.*, 276(33), 31305-31310 (2001)
- [48] F. Meng, F. Sachs, Visualizing dynamic cytoplasmic forces with a compliance-matched FRET sensor, *J. Cell Sci.*, 124(Pt2), 261-269 (2010)
- [49] A. T. Kumar, E. Chung, S.B. Raymond, J. A. Van de Water, K. Shah, D. Fukumura, R. K. Jain, B. J. Bacskai, D. A. Boas, Feasibility of in vivo imaging of fluorescent proteins using lifetime contrast, *Opt. Lett.*, 34(13), 2066-2068 (2009)
- [50] R. H. Berg, R. N. Beachy, Fluorescent protein applications in plants, *Meth. Cell Biol.*, 85,153-177 (2008)
- [51] A. Muñoz-Barrutia, J. García-Muñoz, B. Ucar, I. Fernández-Garúa, C. Ortiz-de-Solorzano, Blind spectral unmixing of M-FISH images by non-negative matrix formation, *Conf. Proc. IEEE Eng. Med. Biol. Soc.*, 6248-6251 (2007)
- [52] J. Walter, B. Joffe, A. Bolzer, H. Albiez, P. A. Benedetti, S. Müller, M. R. Speicher, T. Cremer, M. Cremer, I. Solvei, Towards many colors in FISH on 3D-preserved interphase nuclei, *Cytogenet. Genome Res.* 114 (3-4), 367-378 (2006)
- [53] J. R. Lakowicz, H. Szmanski, K. Nowaczyk, M. L. Johnson, Fluorescence lifetime imaging of free and protein-bound NADH, *PNAS*, 89(4), 1271-1275 (1992)
- [54] E. A. Gibson, O. Masihzadeh, T. C. Lei, D. A. Ammar, M. Y. Kakooch, Multiphoton microscopy for ophthalmic imaging, *J. Ophthalmol.*, 870879 (2011)
- [55] P. Y. Lin, H. C. Lyu, C. Y. S. Hsu, C. S. Chang, F. J. Kao, Imaging dental tissues with multiphoton fluorescence lifetime imaging microscopy, *Biomed. Optics Express*, 2(1), 149-158 (2010)
- [56] J. Phipps, Y. Sun, R. Saroufeem, N. Hatami, M. C. Fishbein, L. Marcu, Fluorescence lifetime imaging for the characterization of the biochemical composition of atherosclerotic plaques, *J. Biomed. Opt.*, 16(9), 096018 (2011)
- [57] J. E. Phipps, Y. sun, M. C. Fishbein, L. Marcu, A fluorescence lifetime imaging classification method to investigate the collagen to lipid ratio in fibrous caps of atherosclerotic plaque, *Lasers Surg. Med.*, 44(7), 564-571 (2012)
- [58] D. Schweitzer, S. Schenke, M. Hammer, F. Schweitzer, S. Jentsch, E. Birckner, W. Becker, A. Bergmann, Towards Metabolic Mapping of the Human Retina, *Microscopy Research and Technique*, 70, 410-419 (2007)
- [59] S. Seidenari, F. Arginelli, S. Bassoli, J. Cautela, P. M. W. French, M. Guanti, D. Guardoli, K. König, C. Talbot, C. Dunsby, Multiphoton Laser Microscopy and Fluorescence Lifetime Imaging for the Evaluation of the Skin, *Dermatology Research and Practice*, 810749 (2012)

- [60] A. Čeklovský, A. Czímerová, K. Lang, J. Budják, Layered silicate films with photochemically active porphyrin cations, *Pure Appl. Chem.*, 81(8), 1385-1396 (2009)
- [61] M. Folmar, T. Shtoyko, R. Fudala, I. Akopova, Z. Gryczynski, S. Raut, I. Gryczynski, Metal Enhanced Fluorescence of Me-ADOTA-Cl Dye by Silver Triangular Nanoprisms on a Gold Film, *Chem. Phys. Lett.*, 531, 126-131 (2012)
- [62] J. H. Huang, F. C. Chen, C. L. Chen, A. T. Huang, Y. S. Hsiao, C. M. Teng, F. W. Yen, P. Chen, C. W. Chu, Molecular-weight-dependent nanoscale morphology in silole-containing cyclopentadithiophene polymer and fullarene derivative blends, *Organics Electronics*, 12, 1755-1762 (2011)
- [63] R. K. Ahrenkiel, N. Call, S. W. Johnston, W. K. Metzger, Comparison of techniques for measuring carrier lifetime in thin-film microcrystalline photovoltaic materials, *Solar Energy Materials & Solar Cells*, 94, 2197-2204 (2010)
- [64] B. M. Keyes, P. Dipko, W. K. Metzger, J. AbuShama, R. Noufi, Changes in the dominant recombination mechanisms of polycrystalline Cu(In, Ga)Se<sub>2</sub> occurring during growth, *J. Appl. Phys.*, 94(9), 5584-5591 (2003)
- [65] W. K. Metzger, D. Albin, D. Levin, P. Sheldon, X. Li, B. M. Keyes, R.K. Ahrenkiel, Time-resolved photoluminescence studies of CdTe, *J. Appl. Phys.* 94, 3549-3555 (2003)
- [66] J. H. Huang, F. C. Chien, P. Chen, K. C. Ho, C. W. Chu, Monitoring the 3D nanostructures of bulk heterojunction polymer solar cells using confocal lifetime imaging, *Anal. Chem.*, 82(5), 1669-1673 (2010)
- [67] K. P. Ghiggino, T. D. M. Bell, E. N. Hooley, Synthetic Polymers for Solar Harvesting, *Faraday Discussions*, 155, 079-088 (2012)
- [68] C. Giansante, G. Raffy, C. Schäfer, H.Rahma, M. T. Kao, A. G. L. Olive, A. Del Guerzo, White-Light-Emitting Self-Assembled NanoFibers and Their Evidence by Microspectroscopy of Individual Objects, *J. Am. Chem. Soc.*, 133, 316-325 (2011)
- [69] V. K. Komarala, C. Xie, Y. Wang, J. Xu, M. Xiao, Time-resolved photoluminescence properties of CuInS<sub>2</sub>/ZnS nanocrystals: Influence of intrinsic defects and external impurities, *J. Appl. Phys.*, 111, 124314 (2012)
- [70] J. W. Grate, R. T. Kelly, J. Suter, N. C. Anheier, Silicon-on-glass pore network micromodels with oxygen-sensing fluorophore films for chemical imaging and defined spatial structure, *Lab Chip*, 12(22), 4796-4801 (2012)
- [71] J. López-Gejo, D. Haigh, G. Orellana, Relationship between the Microscopic and Macroscopic World in Optical Oxygen Sensing: A Luminescence Lifetime Microscopy Study, *Langmuir*, 26(3), 2144-2150 (2010)
- [72] D. Savateeva, D. Melnikau, V. Lesnyak, N. Gaponik, Y. P. Rakovich, Hybrid organic/inorganic semiconductor nanostructures with highly efficient energy transfer, *J. Materials Chem.*, 22, 10816-10820 (2012)
- [73] F. Yang, Z. Xu, J. Wang, F. Zan, C. Dong, J. Ren, Microwave-assisted aqueous synthesis of new quaternary-alloyed CdSeTeS quantum dots; and their bioapplications in targeted imaging of cancer cells, *Luminescence*, DOI: 10.1002/bio.2395 (2012)
- [74] A. Rakovich, D. Savateeva, T. Rakovich, J. F. Donegan, Y. P. Rakovich, V. Kelly, V. Lesnyak, A. Eychmüller, CdTe quantum dot/dye hybrid system as photosensitizer for photodynamic therapy, *Nanoscale Res. Lett.*, 05, 753-760 (2010)
- [75] V. Buschmann, H. Hempel, A. Knigge, C. Kraft, M. Roczen, M. Weyers, T. Siebert, F. Koberling, Characterization of semiconductor devices and wafer materials via sub-nanosecond timecorrelated single photon counting, *Technical Note*
- [76] I. Gregor, B. Krämer, F. Koberling, R. Erdmann, J. Enderlein, M. Wahl, S. Fore, Fast algorithms for the analysis of spectral FLIM data, *Proc. SPIE*, 7903, 790330 (2011)
- [77] M. König, F. Koberling, D. Walters, J. Viani, R. Ros, O. Schulz, Combining Atomic Force Microscopy with confocal Microscopy, *Technical note*, [http://www.picoquant.com/technotes/technote\\_mt200\\_afm.pdf](http://www.picoquant.com/technotes/technote_mt200_afm.pdf) (2009)



PicoQuant GmbH  
 Rudower Chaussee 29 (IGZ)  
 12489 Berlin  
 Germany

Phone +49-(0)30-6392-6929  
 Fax +49-(0)30-6392-6561  
 Email [info@picoquant.com](mailto:info@picoquant.com)  
 WWW <http://www.picoquant.com>

Copyright of this document belongs to PicoQuant GmbH. No parts of it may be reproduced, translated or transferred to third parties without written permission of PicoQuant GmbH. All information given here is reliable to our best knowledge. However, no responsibility is assumed for possible inaccuracies or omissions. Specifications and external appearances are subject to change without notice.

© PicoQuant GmbH, 2013